Dynamic Phase-Field Fracture in Viscoelastic Materials using a First-Order Formulation

Kai Friebertshäuser[3], **Marita Thomas**[1,2], **Sven Tornquist**[2*], **Kerstin Weinberg**[3], and **Christian Wieners**[4]

[1] Weierstrass Institute for Applied Analysis and Stochastics, Berlin, Germany
[2] FU Berlin, Germany
[3] University of Siegen, Germany
[4] Karlsruhe Institute of Technology, Germany

In this contribution we present analytical results on a model for dynamic fracture in viscoelastic materials at small strains that have been obtained in full depth in [1]. In the model, the sharp crack interface is regularized with a phase-field approximation, and for the phase-field variable a viscous evolution with a quadratic dissipation potential is employed. A non-smooth penalization prevents material healing. The viscoelastic momentum balance is formulated as a first order system and coupled in a nonlinear way to the non-smooth evolution equation of the phase field. We give a full discretization in time and space using a discontinuous Galerkin method for the first-order system. We discuss the existence of discrete solutions and, with the step size in space and time tending to zero, their convergence to a suitable notion of weak solution of the system. Eventually, we provide a numerical benchmark and compare it with simulation results found in [2].

1 Introduction

Understanding the dynamics of fracture and damage in deformable solids is an ongoing field of research in engineering sciences and a rigorous mathematical analysis of proposed models is still challenging.
Fracture in a deformable solid appears as a spatial discontinuity in the material domain $\Omega \subset \mathbb{R}^d$, $d \in \{2,3\}$. One well-established concept to overcome inherent numerical and analytical difficulties is to regularize the sharp crack interface with a phase-field approximation. For this, the internal variable $z\colon \Omega \to [0,1]$ is introduced to represent the volume fraction of undamaged material and a variational approach with interacting potential and crack surface energies is followed [3].

Dynamic fracture refers to processes where rapid external loadings are applied to the system or the interplay of elastic wave and crack propagation are too significant to neglect the inertial forces. An illustrative example for the latter phenomenon is the numerical 1D example in Figure 1. Here, a pressure wave is induced from left and right into the sample material, e.g. a thin rod where ends are not fixed. In each picture, the upper plot shows the propagation of the elastic wave marking tensile stress in red and compressive stress in blue. The respective lower plot tracks the damage of the material with 0 for completely damaged and 1 for undamaged material. The reflection at the free boundaries turns pressure into tensile stress in Fig. 1b and by superposition the stress becomes large enough to develop some crack as seen in Fig. 1d-f. The process continues and the waves are reflected at the crack that forms an additional free boundary. In Fig. 1l, again by superposition of waves with different directions, two additional cracks appear in a certain distance on the left and right of the center crack. For this effect, the correct description of the wave propagation is essential. While existence of solutions in such dynamic context has been shown with second-order formulations for the momentum balance (see, e.g., [4–8]), it is known that time discretizations using finite differences or Newmark methods reveal a high numerical dissipation as discussed in [9]

Therefore, to make the numerical implementation robust against spurious energy loss, the viscoelastic momentum balance is reformulated as a first-order system combined with a spatial approximation employing a discontinuous Galerkin method. This method has been developed and tested in [9]. In [1] we provide a mathematical rigorous convergence analysis for the algorithm of [9]. These analytical results we present here in the following.

In this paper, the dynamic fracture is monitored within the time interval $[0,T] \subset \mathbb{R}$ in the domain $\Omega \subset \mathbb{R}^d$, $d \in \{2,3\}$, which represents the viscoelastic material. We introduce the displacement field $\mathbf{u}\colon [0,T] \times \Omega \to \mathbb{R}^d$, the velocity $\mathbf{v} = \partial_t \mathbf{u}$, the linearized strain $\boldsymbol{\varepsilon} = \operatorname{sym}(\mathrm{D}\mathbf{u}) = \frac{1}{2}(\mathrm{D}\mathbf{u} + \mathrm{D}\mathbf{u}^{\mathrm{T}})$ as a measure for the strain for small deformations and the strain rate $\dot{\boldsymbol{\varepsilon}} = \partial_t \boldsymbol{\varepsilon} = \operatorname{sym}(\mathrm{D}\mathbf{v})$ where $\dot{\boldsymbol{\varepsilon}}$ and $\partial_t \boldsymbol{\varepsilon}$ denote the time derivative of $\boldsymbol{\varepsilon}$. With constant material tensors, $\mathbb{C} \in \mathbb{R}^{d\times d\times d\times d}_{\mathrm{sym}}$ the Hookean elasticity tensor, damping tensor $\mathbb{D} \in \mathbb{R}^{d\times d\times d\times d}_{\mathrm{sym}}$ and the degradation function $g \in \mathrm{C}^2(\mathbb{R})$, the degraded viscoelastic stress response is given by $\boldsymbol{\sigma} = g(z)\mathbb{C}\boldsymbol{\varepsilon} + \mathbb{D}\partial_t \boldsymbol{\varepsilon}$. Assuming initial values $\mathbf{u}_0$ and $\boldsymbol{\varepsilon}_0$ with $\boldsymbol{\varepsilon}_0 = \operatorname{sym}(\mathrm{D}\mathbf{u}_0)$, the displacement $\mathbf{u}$ can be recovered such that $\mathbf{u}(t) = \mathbf{u}_0 + \int_0^t \mathbf{v}(s)\,\mathrm{d}s$. Then, the second-order approach in [8] is reformulated with a first-order

* Corresponding author: e-mail sven.tornquist@fu-berlin.de, phone +49 30 838 65259, fax +49 30 838 465259

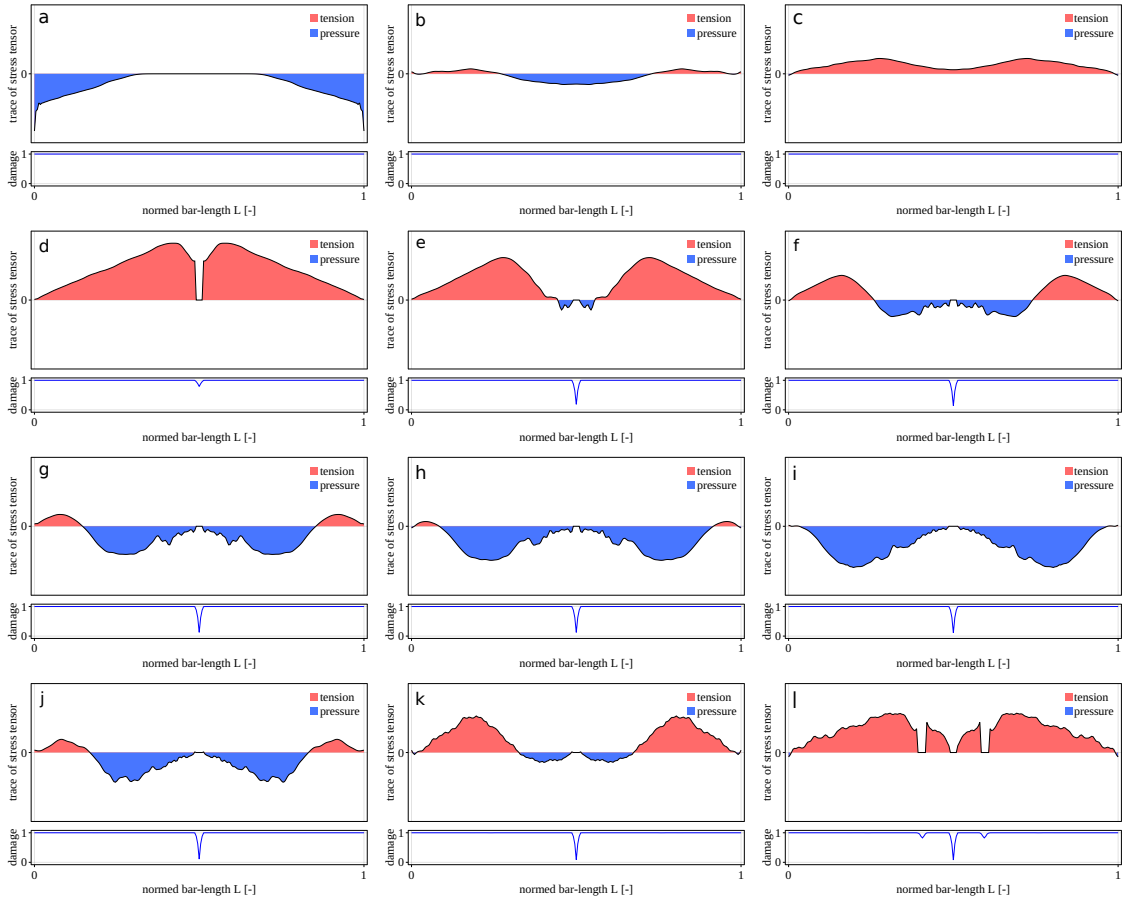

Fig. 1: 1D simulation of crack and elastic wave interplay.

of the momentum balance in terms of state variables $(\mathbf{v}, \boldsymbol{\varepsilon}, \boldsymbol{\sigma})$ as

$$\varrho_0 \partial_t \mathbf{v} - \operatorname{div} \boldsymbol{\sigma} = \mathbf{f}\,, \tag{1a}$$

$$\partial_t \boldsymbol{\varepsilon} - \operatorname{sym}(\mathrm{D}\mathbf{v}) = \mathbf{0}\,, \tag{1b}$$

$$\boldsymbol{\sigma} - g(z)\mathbb{C}\boldsymbol{\varepsilon} - \mathbb{D}\partial_t \boldsymbol{\varepsilon} = \mathbf{0} \tag{1c}$$

with mass density $\varrho_0 > 0$ and volume force density $\mathbf{f}$, compare also to [9]. The analysis includes the case $\mathbb{D} = \mathbf{0}$ without viscosity, but then the regularity of the solution is reduced. To characterize the fraction of damage in a material point, the phase-field variable $z\colon [0,T] \times \Omega \to [0,1]$ is used where $z(t,x) = 1$ stands for completely sound material and $z(t,x) = 0$ for maximal damage. A monotone evolution of the damage variable so that material healing is forbidden, is enforced with the help of the characteristic function

$$\chi_{(-\infty,0]}(\dot{z}) = \begin{cases} \infty & \dot{z} > 0\,, \\ 0 & \dot{z} \le 0\,. \end{cases}$$

This results in a non-smooth evolution law for the phase-field variable in terms of a subdifferential inclusion that reads

$$0 \in \tau_{\mathrm{r}} \partial_t z + \partial \chi_{(-\infty,0]}(\partial_t z) + \frac{1}{2} g'(z) \mathbb{C}\boldsymbol{\varepsilon} : \boldsymbol{\varepsilon} - G_{\mathrm{c}}\big(1 - z + l_{\mathrm{c}}^2 \Delta z\big) \qquad \text{in } (0,T) \times \Omega\,. \tag{2}$$

The phase-field evolution depends on a retardation time $\tau_{\mathrm{r}} > 0$, a length scale $l_{\mathrm{c}} > 0$ and a scaling factor $G_{\mathrm{c}} > 0$. Here, G_{c} depends on the Griffiths constant for brittle fracture and also on the length scale $1/l_{\mathrm{c}}$. In particular, the term $-(1 - z + l_{\mathrm{c}}\Delta z)$ is responsible for the phase-field approximation of the sharp crack surface in the spirit of [10]. The evolution laws (1) and (2) are complemented by initial and boundary conditions on $\partial\Omega = \partial_{\mathrm{N}}\Omega \cup \partial_{\mathrm{D}}\Omega$ with $\partial_{\mathrm{N}}\Omega$ denoting the Neumann and $\partial_{\mathrm{D}}\Omega$ the Dirichlet boundary:

$$\mathbf{v}(0) = \mathbf{v}_0 \ \text{ in } \Omega\,, \qquad \boldsymbol{\varepsilon}(0) = \boldsymbol{\varepsilon}_0 \ \text{ in } \Omega\,, \qquad z(0) = 1 \ \text{ in } \Omega\,,$$

$$\boldsymbol{\sigma}\mathbf{n} = \mathbf{g}_{\mathrm{N}} \text{ on } (0,T) \times \partial_{\mathrm{N}}\Omega\,, \qquad \mathbf{v} = \mathbf{v}_{\mathrm{D}} \text{ on } (0,T) \times \partial_{\mathrm{D}}\Omega\,, \qquad \nabla z \cdot \mathbf{n} = 0 \text{ on } (0,T) \times \partial\Omega$$

with initial data $\mathbf{v}_0$ and $\boldsymbol{\varepsilon}_0$, volume forces $\mathbf{f}$, and boundary data $\mathbf{g}_{\mathrm{N}}$ and $\mathbf{v}_{\mathrm{D}}$.

Structure of the paper. In Sect. 2 the setup of the problem is specified with mathematical assumptions on the domain and given data, and a weak formulation is presented. Sect. 3 introduces the discrete system with a staggered implicit discretization scheme for the time and a discontinuous Galerkin approach for the space which originates in the solution theory of first-order hyperbolic systems. In Sect. 4 analytical results are presented and we refer for the comprehensive proofs to [1]. In 4.1 the existence of discrete solutions is stated. While for the elastic part a linear system of equations has to be solved, the case for the phase-field evolution is more involved and relies on a generalized Newton method with a descent approach to ensure also an energy stability estimate. In Lemma. 4.3, the limit passage is performed and the existence of weak solutions in the sense of Def. 2.1 is concluded in Theorem 4.4.

The terminal section considers the concept of peridynamics that has moved into the focus of engineering applications in the recent past as an alternative to classical continuum mechanics. In our project various alternative concepts for the description of fracture and their compatibility with approximation methods are investigated. In this regard, the approach of peridynamics as continuum-kinematics based peridynamics for the propagation of fracture looks promising [11] and avoids restrictions in the description of material response [12–14]. Thus, we close this manuscript with numerical examples in Sect. 5 comparing the simulation of a curved bar under pressure implemented using the continuum-kinematic based peridynamics (CPD) and the classial continuum mechanics method with a phase-field regularization as described in this manuscript.

2 Mathematical assumptions and weak formulation

In order to present a weak formulation of the momentum balance (1) and the differential inclusion (2), we make the following assumptions.

Assumptions on the domain: We assume that $\Omega \subset \mathbb{R}^d$ for $d \in \{2,3\}$ is a bounded Lipschitz domain with boundary $\partial\Omega = \overline{\Omega} \setminus \Omega$ and relatively open Dirichlet and Neumann boundaries $\partial_{\mathrm{D}}\Omega, \partial_{\mathrm{N}}\Omega \subset \partial\Omega$ such that $\overline{\partial_{\mathrm{D}}\Omega \cup \partial_{\mathrm{N}}\Omega} = \partial\Omega$. We denote by $Q = (0,T) \times \Omega$ the time-space cylinder.

Assumptions on the tensors $\mathbb{C}, \mathbb{D}$ and the degradation function g: The material tensors $\mathbb{C}, \mathbb{D} \in \mathbb{R}^{d\times d\times d\times d}_{\mathrm{sym}}$ are assumed to be positive definite, i.e. $\mathbb{C}\mathbf{A} : \mathbf{A} > 0$ and $\mathbb{D}\mathbf{A} : \mathbf{A} \geq 0$ for $\mathbf{0} \neq \mathbf{A} \in \mathbb{R}^{d\times d}_{\mathrm{sym}}$. The material is degraded by the function $g \in \mathrm{C}^2(\mathbb{R})$ which is monotone $g' \geq 0$ and bounded away from zero $g(0) = g_* > 0$ since we are assuming locally constant growth $g'(z) = 0$ for $z \leq 0$ and $z \geq 2$. Then, $0 < g_* < g^*$ and $g^{**} > 0$ exists such that $0 < g_* \leq g(z) \leq g^*$ and $0 \leq g'(z) \leq g^{**}$, so that $g(z), g(z)^{-1} \in \mathrm{L}^\infty(\Omega)$ for $z \in \mathrm{H}^1(\Omega)$.

Assumptions on the given data: We assume $\mathbf{f} \in \mathrm{L}^2(Q;\mathbb{R}^d)$ for the external volume force in (1a), for the boundary data, $\mathbf{g}_{\mathrm{N}} \in \mathrm{L}^2((0,T)\times\partial_{\mathrm{N}}\Omega;\mathbb{R}^d)$ and $\mathbf{v}_{\mathrm{D}} \in \mathrm{L}^2((0,T)\times\partial_{\mathrm{D}}\Omega;\mathbb{R}^d)$, and for the initial data $\mathbf{v}_0 \in \mathrm{L}^2(\Omega;\mathbb{R}^d)$ and $\boldsymbol{\varepsilon}_0 \in \mathrm{L}^2(\Omega;\mathbb{R}^{d\times d}_{\mathrm{sym}})$. Then, for $Q = (0,T)\times\Omega$ smooth function spaces are introduced

$$
\begin{aligned}
&\mathcal{V} = \mathrm{C}^1(\overline{Q};\mathbb{R}^d)\,, \quad \mathcal{V}_{T,\mathrm{D}} = \big\{\mathbf{w} \in \mathcal{V}\colon \mathbf{w}(T) = \mathbf{0} \text{ in } \Omega\,,\ \mathbf{w} = \mathbf{0} \text{ on } (0,T)\times\Gamma_{\mathrm{D}}\big\}\,,\\
&\mathcal{W} = \mathrm{C}^1(\overline{Q};\mathbb{R}^{d\times d}_{\mathrm{sym}})\,, \quad \mathcal{W}_T = \big\{\boldsymbol{\Phi} \in \mathcal{W}\colon \boldsymbol{\Phi}(T) = \mathbf{0} \text{ in } \Omega\big\}\,,\\
&\mathcal{W}_{T,\mathrm{N}} = \big\{\boldsymbol{\Psi} \in \mathcal{W}_T\colon \boldsymbol{\Psi}\mathbf{n} = \mathbf{0} \text{ on } (0,T)\times\Gamma_{\mathrm{N}}\big\}\,, \quad \mathcal{Z} = \big\{\varphi \in \mathrm{C}^1(\overline{Q})\colon \varphi \leq 0 \text{ a.e. in } Q\big\}\,.
\end{aligned}
$$

In addition, we set

$$
\begin{aligned}
&m_Q\big((\mathbf{v},\boldsymbol{\varepsilon}),(\mathbf{w},\boldsymbol{\eta})\big) = \big(\varrho_0\mathbf{v},\mathbf{w}\big)_Q + \big(\boldsymbol{\varepsilon},\boldsymbol{\eta}\big)_Q\,,\ a_Q\big((\mathbf{v},\boldsymbol{\sigma}),(\mathbf{w},\boldsymbol{\Phi})\big) = \big(\boldsymbol{\sigma},\mathrm{sym}(\mathrm{D}\mathbf{w})\big)_Q + \big(\mathbf{v},\operatorname{div}\boldsymbol{\Phi}\big)_Q\,,\\
&r_Q\big(z;(\boldsymbol{\varepsilon},\boldsymbol{\sigma}),\boldsymbol{\Psi}\big) = \big(\boldsymbol{\sigma} - g(z)\mathbb{C}\boldsymbol{\varepsilon},\boldsymbol{\Psi}\big)_Q\,,\ b_Q(z,\varphi) = -G_{\mathrm{c}}\big(1-z,\varphi\big)_Q + G_{\mathrm{c}}l_{\mathrm{c}}^2\big(\nabla z,\nabla\varphi\big)_Q \quad \text{and}\\
&\ell_Q(\mathbf{w},\boldsymbol{\Phi},\boldsymbol{\Psi}) = \big(\mathbf{f},\mathbf{w}\big)_Q + \big(\varrho_0\mathbf{v}_0,\mathbf{w}(0)\big)_\Omega + \big(\boldsymbol{\varepsilon}_0,\boldsymbol{\Phi}(0) - \mathbb{D}\boldsymbol{\Psi}(0)\big)_\Omega + \big(\mathbf{v}_{\mathrm{D}},\boldsymbol{\Phi}\mathbf{n}\big)_{(0,T)\times\Gamma_{\mathrm{D}}} + \big(\mathbf{g}_{\mathrm{N}},\mathbf{w}\big)_{(0,T)\times\Gamma_{\mathrm{N}}}
\end{aligned}
$$

where $(\cdot,\cdot)_Q$ denotes the inner product on $\mathrm{L}^2(Q)$, $\mathrm{L}^2(Q;\mathbb{R}^d)$ or $\mathrm{L}^2(Q;\mathbb{R}^{d\times d}_{\mathrm{sym}})$ depending on the respective arguments. Here, in the last line, the form ℓ_Q depends on the data $\mathbf{f}$, $\mathbf{v}_0$, $\boldsymbol{\varepsilon}_0$, $\mathbf{v}_{\mathrm{D}}$, and $\mathbf{g}_{\mathrm{N}}$.

A variational characterization of the elastic system in (1) is found by testing with smooth test functions $(\mathbf{w},\boldsymbol{\Phi},\boldsymbol{\Psi}) \in \mathcal{V}_{T,\mathrm{D}} \times \mathcal{W}_{T,\mathrm{N}} \times \mathcal{W}_T$ and integrating by parts to shift all derivatives to the test functions. Similar one proceeds for the phase-field evolution in (2) and a suitable weak formulation for the system is given by:

Definition 2.1 (Weak solution) The triple $(\mathbf{v},\boldsymbol{\varepsilon},\boldsymbol{\sigma}) \in \mathrm{L}^2(Q;\mathbb{R}^d\times\mathbb{R}^{d\times d}_{\mathrm{sym}}\times\mathbb{R}^{d\times d}_{\mathrm{sym}})$ and $z \in \mathrm{H}^1(0,T;\mathrm{L}^2(\Omega))\cap\mathrm{L}^2(0,T;\mathrm{H}^1(\Omega))$ with $z(0) = 1$ in Ω is a weak solution of the system (1), (2) if for all smooth test functions $(\mathbf{w},\boldsymbol{\Phi},\boldsymbol{\Psi}) \in \mathcal{V}_{T,\mathrm{D}} \times \mathcal{W}_{T,\mathrm{N}} \times \mathcal{W}_T$ and $\varphi \in \mathcal{Z}$ it is satisfied

$$
-m_Q\big((\mathbf{v},\boldsymbol{\varepsilon}),(\partial_t\mathbf{w},\partial_t\boldsymbol{\Phi} - \mathbb{D}\partial_t\boldsymbol{\Psi})\big) + a_Q\big((\mathbf{v},\boldsymbol{\sigma}),(\mathbf{w},\boldsymbol{\Phi})\big) + r_Q\big(z;(\boldsymbol{\varepsilon},\boldsymbol{\sigma}),\boldsymbol{\Psi}\big) - \ell_Q(\mathbf{w},\boldsymbol{\Phi},\boldsymbol{\Psi}) = 0\,, \tag{5a}
$$

$$
\tau_{\mathrm{r}}\big(\partial_t z,\varphi\big)_Q + \frac{1}{2}\big(g'(z)\mathbb{C}\boldsymbol{\varepsilon} : \boldsymbol{\varepsilon},\varphi\big)_Q + b_Q(z,\varphi) \geq 0\,. \tag{5b}
$$

If $\mathbb{D}$ is positive definite, also an energy-dissipation inequality holds true, i.e.,

$$\begin{aligned}\mathcal{E}^{\mathrm{kin}}\big(\mathbf{v}(t)\big) + \mathcal{E}^{\mathrm{el}}\big(z(t),\boldsymbol{\varepsilon}(t)\big) + \mathcal{E}^{\mathrm{pf}}\big(z(t)\big) + \int_0^t 2\mathcal{R}^{\mathrm{vis}}(\partial_s\boldsymbol{\varepsilon}) + \mathcal{R}^{\mathrm{pf}}(\partial_s z)\,\mathrm{d}s \\ \leq \mathcal{E}^{\mathrm{kin}}\big(\mathbf{v}(0)\big) + \mathcal{E}^{\mathrm{el}}\big(z(0),\boldsymbol{\varepsilon}(0)\big) + \mathcal{E}^{\mathrm{pf}}\big(z(0)\big) + \int_0^t \mathcal{E}^{\mathrm{ext}}\big(s,\mathbf{v}(s)\big)\,\mathrm{d}s\,.\end{aligned} \tag{5c}$$

Above, in (5c) we have used the following notation for the energy functionals and dissipation potentials in the system:

$$\mathcal{E}^{\mathrm{el}}(z,\boldsymbol{\varepsilon}) = \int_\Omega \frac{1}{2}g(z)\mathbb{C}\boldsymbol{\varepsilon}:\boldsymbol{\varepsilon}\,\mathrm{d}\mathbf{x}\,,\quad \mathcal{E}^{\mathrm{pf}}(z) = \frac{G_{\mathrm{c}}}{2}\int_\Omega \big((1-z)^2 + l_{\mathrm{c}}^2|\nabla z|^2\big)\,\mathrm{d}\mathbf{x}\,,\quad \mathcal{E}^{\mathrm{kin}}(\mathbf{v}) = \frac{\varrho_0}{2}\int_\Omega |\mathbf{v}|^2\,\mathrm{d}\mathbf{x}\,, \tag{6}$$

$$\mathcal{E}^{\mathrm{ext}}(t,\mathbf{v}) = \int_\Omega \mathbf{f}(t)\cdot\mathbf{v}\,\mathrm{d}\mathbf{x} + \int_{\partial_{\mathrm{N}}\Omega}\mathbf{g}_{\mathrm{N}}(t)\cdot\mathbf{v}\,\mathrm{d}\mathbf{x}\,,\quad \mathcal{R}^{\mathrm{vis}}(\dot{\boldsymbol{\varepsilon}}) = \int_\Omega \frac{1}{2}\mathbb{D}\dot{\boldsymbol{\varepsilon}}:\dot{\boldsymbol{\varepsilon}}\,\mathrm{d}\mathbf{x}\,,\quad \mathcal{R}^{\mathrm{pf}}(\dot z) = \int_\Omega \frac{\tau_{\mathrm{r}}}{2}|\dot z|^2 + \chi_{(-\infty,0]}(\dot z)\,\mathrm{d}\mathbf{x}\,.$$

In the quadratic potential $\mathcal{E}^{\mathrm{el}}$ the phase field z and the strain $\boldsymbol{\varepsilon}$ are coupled in a nonlinear way through the degradation function g: Elastic forces are small in regions where the damage is large. The functional $\mathcal{E}^{\mathrm{pf}}$ is of Modica-Mortola type and approximates the sharp crack interface , and $\mathcal{R}^{\mathrm{vis}}$ is a viscous dissipation potential depending on the strain rate $\dot{\boldsymbol{\varepsilon}}$. The second summand in the quadratic dissipation potential $\mathcal{R}^{\mathrm{pf}}$ imposes the monotonicity constraint for the phase-field variable z.

3 Discrete System

A weak solution in the sense of Definition 2.1 is approximated by a fully discrete scheme in space and time.

Approximation in space The viscoelastic wave equation is approximated with a discontinuous Galerkin (DG) method and the phase field with lowest order conforming finite elements. On a mesh $\Omega_h = \bigcup_{K\in\mathcal{K}_h} K$ with (open) cells K, let $V_h^{\mathrm{dg}} = \prod_{K\in\mathcal{K}_h}\mathbb{P}_k(K;\mathbb{R}^d)$ and $W_h^{\mathrm{dg}} = \prod_{K\in\mathcal{K}_h}\mathbb{P}_k(K;\mathbb{R}^{d\times d}_{\mathrm{sym}})$ be the discontinuous finite element space of polynomial degree $k\geq 1$, and let $V_h^{\mathrm{cf}}\subset\mathbb{P}(\Omega_h)\cap\mathrm{C}^0(\overline{\Omega})$ be the lowest order conforming finite elements. We assume that the mesh is shape regular and that $\mathrm{diam}(K)\leq h$ for $K\in\mathcal{K}_h$. The DG approximation of the discontinuous functions $(\mathbf{v}_h,\boldsymbol{\sigma}_h),(\mathbf{w}_h,\boldsymbol{\Phi}_h)\in V_h^{\mathrm{dg}}\times W_h^{\mathrm{dg}}$ is attained by solving a Riemann problem locally between faces of neighbouring finite element cells to find a good approximation for the crossing flux (see details in [1], derivation for linear elasticity in [15, 16]). Depending on the phase field $z_h\in V_h^{\mathrm{cf}}$ the operators

$$a_h^{\mathrm{dg}}\big(z_h;(\mathbf{v}_h,\boldsymbol{\sigma}_h),(\mathbf{w}_h,\boldsymbol{\Phi}_h)\big) = \big(\boldsymbol{\sigma}_h,\mathrm{sym}(\mathrm{D}\mathbf{w}_h)\big)_{\Omega_h} + \big(\mathbf{v}_h,\mathrm{div}\,\boldsymbol{\Phi}_h\big)_{\Omega_h} + \textbf{[jump terms]} \tag{7}$$

$$\ell_h^{\mathrm{dg}}\big(t,z_h;(\mathbf{w}_h,\boldsymbol{\Phi}_h)\big) = \big(\mathbf{f}(t),\mathbf{w}_h\big)_\Omega + \big(\mathbf{v}_{\mathrm{D}}(t),\boldsymbol{\Phi}_h\mathbf{n}\big)_{\Gamma_{\mathrm{D}}} + \big(\mathbf{g}_{\mathrm{N}}(t),\mathbf{w}_h\big)_{\Gamma_{\mathrm{N}}} + \textbf{[jump terms]} \tag{8}$$

are defined that provide two main features used in the analysis: *Monotonicity*, that is $a_h^{\mathrm{dg}}\big(z_h;(\mathbf{v}_h,\boldsymbol{\sigma}_h),(\mathbf{v}_h,\boldsymbol{\sigma}_h)\big)\geq 0$ and *consistency*, i.e. for smooth test functions $(\mathbf{w},\boldsymbol{\Phi})\in\mathcal{V}_{T,\mathrm{D}}\times\mathcal{W}_{\mathrm{N}}$ and $t\in(0,T)$ it is

$$\begin{aligned}a_h^{\mathrm{dg}}\big(z_h;(\mathbf{v}_h,\boldsymbol{\sigma}_h),(\mathbf{w},\boldsymbol{\Phi})(t)\big) &= \big(\boldsymbol{\sigma}_h,\mathrm{sym}(\mathrm{D}\mathbf{w})(t)\big)_\Omega + \big(\mathbf{v}_h,\mathrm{div}\,\boldsymbol{\Phi}(t)\big)_\Omega\,,\\ \ell_h^{\mathrm{dg}}\big(t,z_h;(\mathbf{w},\boldsymbol{\Phi})(t)\big) &= \big(\mathbf{f}(t),\mathbf{w}\big)_\Omega + \big(\mathbf{v}_{\mathrm{D}}(t),\boldsymbol{\Phi}(t)\mathbf{n}\big)_{\Gamma_{\mathrm{D}}} + \big(\mathbf{g}_{\mathrm{N}}(t),\mathbf{w}(t)\big)_{\Gamma_{\mathrm{N}}}\,.\end{aligned}$$

Approximation in time In the time-discrete formulation, the non-smooth constraint $\partial_t z\leq 0$ is approximated using a Yosida regularization $(\theta_h/2)M_+^2(\dot z)$ defined by $M_+(\dot z)=\max\{\dot z,0\}$ and a penalty parameter $\theta_h>0$ s.t. $\theta_h\to\infty$ as $h\to 0$. With this, a regularization of the viscous dissipation potential for the phase field, $\mathcal{R}^{\mathrm{pf}}$ from (6), is given by

$$\mathcal{R}_h^{\mathrm{pf}}(\dot z) = \int_\Omega\left(\frac{\tau_{\mathrm{r}}}{2}|\dot z|^2 + \frac{\theta_h}{2}M_+^2(\dot z)\right)\mathrm{d}\mathbf{x}\,,$$

and we set

$$\begin{aligned}m_\Omega\big((\mathbf{v},\boldsymbol{\varepsilon}),(\mathbf{w},\boldsymbol{\eta})\big) &= \big(\varrho_0\mathbf{v},\mathbf{w}\big)_\Omega + \big(\boldsymbol{\varepsilon},\boldsymbol{\eta}\big)_\Omega\,,\quad \mathbf{v},\mathbf{w}\in\mathrm{L}^2(\Omega;\mathbb{R}^d)\,,\quad \boldsymbol{\varepsilon},\boldsymbol{\eta}\in\mathrm{L}^2(\Omega;\mathbb{R}^{d\times d}_{\mathrm{sym}})\,,\\ r_\Omega\big(z;(\boldsymbol{\varepsilon},\boldsymbol{\sigma}),\boldsymbol{\Psi}\big) &= \big(\boldsymbol{\sigma}-g(z)\mathbb{C}\boldsymbol{\varepsilon},\boldsymbol{\Psi}\big)_\Omega\,,\quad z\in\mathrm{L}^\infty(\Omega)\,,\quad \boldsymbol{\sigma},\boldsymbol{\varepsilon},\boldsymbol{\Psi}\in\mathrm{L}^2(\Omega;\mathbb{R}^{d\times d}_{\mathrm{sym}})\,,\\ b_\Omega(z,\varphi) &= -G_{\mathrm{c}}\big((1-z),\varphi\big)_\Omega + G_{\mathrm{c}}l_{\mathrm{c}}^2\big(\nabla z,\nabla\varphi\big)_\Omega\,,\quad z,\varphi\in\mathrm{H}^1(\Omega)\,.\end{aligned}$$

Depending on $z_h^{n-1}\in V_h^{\mathrm{cf}}$ and $\boldsymbol{\varepsilon}_h^{n-1}$, we define the coercive functional

$$\mathcal{G}_h^n(z_h) = \int_\Omega\Big(\frac{\tau_{\mathrm{r}}}{2\triangle t_h^n}\big(z_h-z_h^{n-1}\big)^2 + \frac{\theta_h}{2\,\triangle t_h^n}M_+^2\big(z_h-z_h^{n-1}\big) + \frac{1}{2}g(z_h)\mathbb{C}\boldsymbol{\varepsilon}_h^{n-1}:\boldsymbol{\varepsilon}_h^{n-1} + \frac{G_{\mathrm{c}}}{2}\big((1-z_h)^2+l_{\mathrm{c}}^2|\nabla z_h|^2\big)\Big)\,\mathrm{d}\mathbf{x}\,.$$

For convience of the presentation uniform time steps $\triangle t_h^n = \triangle t_h = T/N_h$ with $N_h\in\mathbb{N}$ and $N_h\to\infty$ as $h\to 0$ are employed. We set $t_h^0=0$, $t_h^n = n\triangle t_h$ and choose initial values $(\mathbf{v}_h^0,\boldsymbol{\varepsilon}_h^0,\boldsymbol{\sigma}_h^0)\in V_h^{\mathrm{dg}}\times W_h^{\mathrm{dg}}\times W_h^{\mathrm{dg}}$ and $1=z_h^0\in V_h^{\mathrm{cf}}$ i.e. the material without fracture. For every time step $n=1,2,3,\ldots$ a staggered time-discrete scheme is introduced as follows:

(S1) Depending on $(\boldsymbol{\varepsilon}_h^{n-1}, z_h^{n-1})$, approximate the phase field $z_h^n \in V_h^{\mathrm{cf}}$ by solving the nonlinear equation

$$\frac{\tau_{\mathrm{r}}}{\triangle t_h^n}\big(z_h^n - z_h^{n-1}, \varphi_h\big)_\Omega + \frac{\theta_h}{2\,\triangle t_h^n}\big(\frac{\mathrm{d}}{\mathrm{d}z}M_+^2(z_h^n - z_h^{n-1}), \varphi_h\big)_\Omega + \frac{1}{2}\big(g'(z_h^n)\mathbb{C}\boldsymbol{\varepsilon}_h^{n-1} : \boldsymbol{\varepsilon}_h^{n-1}, \varphi_h\big)_\Omega + b_\Omega(z_h^n, \varphi_h) = 0\,,$$

for $\varphi_h \in V_h^{\mathrm{cf}}$ such that $\mathcal{G}_h^n(z_h^n) \le \mathcal{G}_h^n(z_h^{n-1})$; this can be achieved by starting the iterative solution method with z_h^{n-1}.

(S2) Depending on $(\mathbf{v}_h^{n-1}, \boldsymbol{\varepsilon}_h^{n-1}, \boldsymbol{\sigma}_h^{n-1})$ and z_h^n, solve for $(\mathbf{v}_h^n, \boldsymbol{\varepsilon}_h^n, \boldsymbol{\sigma}_h^n) \in V_h^{\mathrm{dg}} \times W_h^{\mathrm{dg}} \times W_h^{\mathrm{dg}}$ the linear equation

$$\begin{aligned} &m_\Omega\big((\mathbf{v}_h^n, \boldsymbol{\varepsilon}_h^n), (\mathbf{w}_h, \boldsymbol{\Phi}_h - \mathbb{D}\boldsymbol{\Psi}_h)\big) + \triangle t_h^n a_h^{\mathrm{dg}}\big(z_h^n; (\mathbf{v}_h^n, \boldsymbol{\sigma}_h^n), (\mathbf{w}_h, \boldsymbol{\Phi}_h)\big) + \triangle t_h^n r_\Omega\big(z_h^n; (\boldsymbol{\varepsilon}_h^n, \boldsymbol{\sigma}_h^n), \boldsymbol{\Psi}_h\big) \\ &\quad = m_\Omega\big(\mathbf{v}_h^{n-1}, \boldsymbol{\varepsilon}_h^{n-1}), (\mathbf{w}_h, \boldsymbol{\Phi}_h - \mathbb{D}\boldsymbol{\Psi}_h)\big) + \triangle t_h^n \ell_h^{\mathrm{dg}}\big(t_h^n, z_h^n; (\mathbf{w}_h, \boldsymbol{\Phi}_h)\big)\,, \quad (\mathbf{w}_h, \boldsymbol{\Phi}_h, \boldsymbol{\Psi}_h) \in V_h^{\mathrm{dg}} \times W_h^{\mathrm{dg}} \times W_h^{\mathrm{dg}}\,. \end{aligned}$$

For simplicity of the presentation, we consider in the following only the case of homogeneous boundary data $\mathbf{v}_{\mathrm{D}} = \mathbf{0}$ and $\mathbf{g}_{\mathrm{N}} = \mathbf{0}$. The volume forces are approximated by the L^2 projection $\mathbf{f}_h^n \in V_h^{\mathrm{dg}}$ in $(t_h^{n-1}, t_h^n) \times \Omega$ while $(\mathbf{v}_h^0, \boldsymbol{\varepsilon}_h^0)$ are the L^2 projections of the initial values $(\mathbf{v}_0, \boldsymbol{\varepsilon}_0)$. Note that in [1] a variable time step is discussed where the step size is adjusted depending on the energy release, see also [9, Elastic time step, Dissipative time step, p. 6].

4 Analytical results

The following results are presented here without proofs. The detailed arguments can be found in [1]. At first, we introduce the notation $\triangle\boldsymbol{\varepsilon}_h^n = \boldsymbol{\varepsilon}_h^n - \boldsymbol{\varepsilon}_h^{n-1}$ and $\triangle z_h^n = z_h^n - z_h^{n-1}$ and define interpolants $(z_h, \mathbf{v}_h, \boldsymbol{\varepsilon}_h, \boldsymbol{\sigma}_h) \in \mathrm{L}^2(0,T; V_h^{\mathrm{cf}} \times V_h^{\mathrm{dg}} \times W_h^{\mathrm{dg}} \times W_h^{\mathrm{dg}})$ by $(z_h, \mathbf{v}_h, \boldsymbol{\varepsilon}_h, \boldsymbol{\sigma}_h)(t) = (z_h^n, \mathbf{v}_h^n, \boldsymbol{\varepsilon}_h^n, \boldsymbol{\sigma}_h^n)$ in (t_h^{n-1}, t_h^n) and $(\dot{z}_h, \dot{\boldsymbol{\varepsilon}}_h) \in \mathrm{L}^2(0,T; V_h^{\mathrm{cf}} \times W_h^{\mathrm{dg}})$ by $(\dot{z}_h, \dot{\boldsymbol{\varepsilon}}_h)(t) = \frac{1}{\triangle t_h^n}(\triangle z_h^n, \triangle\boldsymbol{\varepsilon}_h^n)$ for $t \in (t_h^{n-1}, t_h^n)$.

To establish existence of discrete solutions, for (S2) a linear system of equations has to be solved while the damage evolution (S1) is more involved due to the nonlinearities coming from the Yosida term and the z-dependence of the elastic term.

Lemma 4.1 (Existence of discrete solutions) *Let the assumptions stated in Sect. 2 hold true. Then, for every $n = 1, \dots, N$ and $N \in \mathbb{N}$ there exists a solution $z_h^n \in V_h^{\mathrm{cf}}$ of the nonlinar problem* (S1) *and a unique solution $(\mathbf{v}_h^n, \boldsymbol{\varepsilon}_h^n, \boldsymbol{\sigma}_h^n) \in V_h^{\mathrm{dg}} \times W_h^{\mathrm{dg}} \times W_h^{\mathrm{dg}}$ in* (S2)*. In case of homogeneous boundary data $\mathbf{v}_{\mathrm{D}} = \mathbf{0}$, $\mathbf{g}_{\mathrm{N}} = \mathbf{0}$, the discrete solution is bounded by the discrete energy-dissipation inequality*

$$\begin{aligned} &\mathcal{E}^{\mathrm{kin}}(\mathbf{v}_h^n) + \mathcal{E}^{\mathrm{el}}(z_h^n, \boldsymbol{\varepsilon}_h^n) + \mathcal{E}^{\mathrm{pf}}(z_h^n) + \sum_{k=1}^n \left(\frac{2}{\triangle t_k}\mathcal{R}^{\mathrm{vis}}(\triangle\boldsymbol{\varepsilon}_h^k) + \frac{1}{\triangle t_k}\mathcal{R}_h^{\mathrm{pf}}(\triangle z_h^k)\right) \\ &\qquad \le \mathcal{E}^{\mathrm{kin}}(\mathbf{v}_h^0) + \mathcal{E}^{\mathrm{el}}(z_h^0, \boldsymbol{\varepsilon}_h^0) + \mathcal{E}^{\mathrm{pf}}(z_h^0) + \sum_{k=1}^n \triangle t_k\big(\mathbf{f}_h^k, \mathbf{v}_h^k\big)_\Omega\,. \end{aligned} \tag{10}$$

From the discrete energy-dissipation inequality the following uniform bounds can be deduced:

Lemma 4.2 (Uniform bounds) *Let the assumptions of Lemma 4.1 hold true. Then, for all $h > 0$ the discrete solution $(z_h, \mathbf{v}_h, \boldsymbol{\varepsilon}_h, \dot{z}_h, \mathbb{D}^{1/2}\dot{\boldsymbol{\varepsilon}}_h)$ is uniformly bounded in $Q = (0,T) \times \Omega$ by*

$$\begin{aligned} &\frac{\varrho_0}{4}\big\|\mathbf{v}_h\big\|_Q^2 + \frac{1}{2}\big\|g(z_h)^{1/2}\mathbb{C}^{1/2}\boldsymbol{\varepsilon}_h\big\|_Q^2 + \frac{G_{\mathrm{c}}}{2}\Big(\big\|1 - z_h\big\|_Q^2 + l_c^2\,\big\|\nabla z_h\big\|_Q^2\Big) + \big\|\mathbb{D}^{1/2}\dot{\boldsymbol{\varepsilon}}_h\big\|_Q^2 + \frac{\tau_r}{2}\big\|\dot{z}_h\big\|_Q^2 \\ &\quad + \frac{\theta_h}{2}\big\|\max\{\dot{z}_h, 0\}\big\|_Q^2 \le \max\{T,1\}\Big(\mathcal{E}^{\mathrm{kin}}(\mathbf{v}_h^0) + \mathcal{E}^{\mathrm{el}}(z_h^0, \boldsymbol{\varepsilon}_h^0) + \mathcal{E}^{\mathrm{pf}}(z_h^0)\Big) + \frac{\max\{T,1\}^2}{\varrho_0}\big\|\mathbf{f}\big\|_Q^2\,. \end{aligned}$$

We consider a shape-regular family $\big(\Omega_h\big)_{h\in\mathcal{H}}$ of meshes with $0 \in \overline{\mathcal{H}}$. By the uniform bounds in Lemma 4.2 and standard compactness arguments we can investigate the limit process as $h \to 0$.

Lemma 4.3 *Given the assumptions of Lemma 4.2, there exists a weakly converging subsequence $(z_h, \mathbf{v}_h, \boldsymbol{\varepsilon}_h, \dot{z}_h, \mathbb{D}^{1/2}\dot{\boldsymbol{\varepsilon}}_h)_{h\in\mathcal{H}_0}$ with $\mathcal{H}_0 \subset \mathcal{H}$ and $0 \in \overline{\mathcal{H}}_0$. For the limit*

$$(z, \mathbf{v}, \boldsymbol{\varepsilon}, \dot{z}, \mathbb{D}^{1/2}\dot{\boldsymbol{\varepsilon}}) \in \mathrm{L}^2\big(0,T; \mathrm{H}^1(\Omega)\big) \times \mathrm{L}^2(Q;\mathbb{R}^d) \times \mathrm{L}^2(Q;\mathbb{R}^{d\times d}_{\mathrm{sym}}) \times \mathrm{L}^2(Q) \times \mathrm{L}^2(Q;\mathbb{R}^{d\times d}_{\mathrm{sym}})\,,$$

the weak derivative $\partial_t z$ exists, and we have $z \in \mathrm{H}^1\big(0,T; \mathrm{L}^2(\Omega)\big)$ with $z(0) = z_0$, $\partial_t z = \dot{z} \le 0$ a.e. in Q.
If, in addition, $\mathbb{D}$ is positive definite, also the weak derivatives $\partial_t\boldsymbol{\varepsilon}$ and $\mathrm{sym}(\mathrm{D}\mathbf{v})$ exist, and it is $\partial_t\boldsymbol{\varepsilon} = \dot{\boldsymbol{\varepsilon}} = \mathrm{sym}(\mathrm{D}\mathbf{v})$.

Using a generalized Aubins-Lions statement [17, Lemma 7.7, p. 194], Lemma 4.2 and 4.3 imply strong convergence $z_h \to z$ in $\mathrm{L}^2(Q)$ for the phase-field variable and thus allow to pass to the limit in (S1). In particular one can conclude that $(\boldsymbol{\sigma}_h)_{h\in\mathcal{H}_0}$ converges weakly to $\boldsymbol{\sigma} = g(z)\mathbb{C}\boldsymbol{\varepsilon} + \mathbb{D}\partial_t\boldsymbol{\varepsilon}$ in $\mathrm{L}^2(Q;\mathbb{R}^{d\times d}_{\mathrm{sym}})$ and the limit passage in (S2) is clear. Moreover, for positive definite $\mathbb{D}$ a discrete Aubin-Lions compactness result in [18] enables to find that the extracted limit $(z, \mathbf{v}, \boldsymbol{\varepsilon}, \boldsymbol{\sigma})$ also satisfies the energy-dissipation inequality (5c). Alltogether it follows the existence of solutions in the sense of Def. 2.1.

Theorem 4.4 (Existence of weak solutions) *Let the assumptions of Lemma 4.1 be satisfied. The weak limit $(z, \mathbf{v}, \boldsymbol{\varepsilon}, \boldsymbol{\sigma}) \in \mathrm{H}^1(0,T; \mathrm{L}^2(\Omega)) \cap \mathrm{L}^2(0,T; \mathrm{H}^1(\Omega)) \times \mathrm{L}^2(Q;\mathbb{R}^d) \times \mathrm{L}^2(Q;\mathbb{R}^{d\times d}_{\mathrm{sym}}) \times \mathrm{L}^2(Q;\mathbb{R}^{d\times d}_{\mathrm{sym}})$ of the sequence $(z_h, \mathbf{v}_h, \boldsymbol{\varepsilon}_h, \boldsymbol{\sigma}_h)_{h\in\mathcal{H}_0}$ is a solution of the weak formulation* (5).

5 Numerical examples

We here present a 2D numerical experiment: Similar to the 1D example in the introduction, a curved bar is exposed to pressure waves from left and right, see Fig. 2. Superposition of waves inside the material leads to the formation of a crack, see Fig. 2 a, c. The rupture triggers new waves propagating through the material. These waves again superpose, the same effect as before arises and further cracks are formed, as can be seen in Fig. 2 b, d. Figure 2 a, b shows the damage distribution obtained by the FE-approach discussed in the preceding sections. In the numerical experiment the evolution of the phase filed was implemented using a maximum principal stress criterion. For comparison we also provide in Fig. 2 c, d the results of the experiment simulated with continuum-kinematics based peridynamics approach that was introduced in [12–14] and we also refer to [2]. Both numerical methods qualitatively capture the features of the experiment well. In particular fracture initiates and propagates in the same, physically expected regions of the bar.

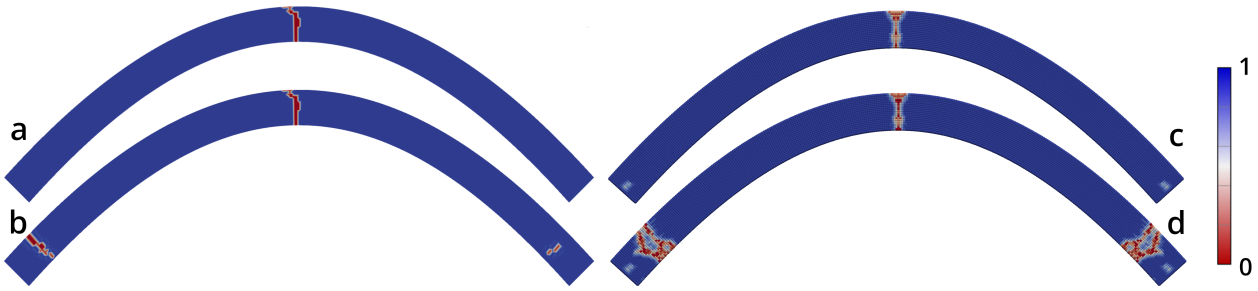

Fig. 2: Damage of a 2d curved bar; a, b: FE-approach; c, d: continuum-kinematics based peridynamics. The setup for the benchmark including loading conditions and material parameters is given in [9] for the FE-approach and in [11] for the continuum-kinematics based peridynamics approach.

Acknowledgements This work is financially supported by the German Research Foundation (DFG) in the priority programme "Variational Methods for Predicting Complex Phenomena in Engineering Structures and Materials" (SPP2256) within the project "Nonlinear Fracture Dynamics: Modeling, Analysis, Approximation, and Applications" (TH 1935/5-1, WE 2525/15-1 and WI 1430/9-1).

References

[1] M. Thomas, S. Tornquist, K. Weinberg, and C. Wieners, Approximating dynamic phase-field fracture in viscoelastic materials with a first-order formulation for velocity and stress, 2022, http://www.wias-berlin.de/projects/SPP2256-19/thomas2022approximating.pdf.
[2] K. Friebertshäuser, M. Thomas, S. Tornquist, C. Wieners, and K. Weinberg, submitted to PAMM (2022).
[3] B. Bourdin, G. Francfort, and J. J. Marigo, Journal of elasticity **91**(1-3), 5–148 (2008).
[4] C. J. Larsen, C. Ortner, and E. Süli, Mathematical Models and Methods in Applied Sciences **20**(07), 1021–1048 (2010).
[5] R. Rossi and M. Thomas, Math. Models Methods Appl. Sci. **27**(08), 1489–1546 (2017).
[6] G. Lazzaroni, R. Rossi, M. Thomas, and R. Toader, Journal of Dynamics and Differential Equations **30**(3), 1311–1364 (2018).
[7] T. Roubíček, Models of dynamic damage and phase-field fracture, and their various time discretisations, in: Topics in Applied Analysis and Optimisation, (Springer, 2019), pp. 363–396.
[8] M. Thomas and S. Tornquist, Discrete & Continuous Dynamical Systems-S **14**(11), 3865–3924 (2021).
[9] K. Weinberg and C. Wieners, Computer Methods in Applied Mechanics and Engineering (CMAME) p. 114330 (2021).
[10] L. Ambrosio and V. M. Tortorelli, Communications on Pure and Applied Mathematics **43**(8), 999–1036 (1990).
[11] K. Friebertshäuser, C. Wieners, and K. Weinberg, AIMS Material Science (to appear) (2022).
[12] A. Javili, A. McBride, and P. Steinmann, Journal of the Mechanics and Physics of Solids **131**(07) (2019).
[13] A. Javili, S. Firooz, A. McBride, and P. Steinmann, Computational Mechanics **66**(10) (2020).
[14] A. Javili, A. McBride, and P. Steinmann, Theoretical and Applied Fracture Mechanics **111**(02), 102850 (2021).
[15] M. Hochbruck, T. Pažur, A. Schulz, E. Thawinan, and C. Wieners, ZAMM **95**(3), 237–259 (2015).
[16] W. Dörfler and C. Wieners, Space-time approximations for linear acoustic, elastic, and electro- magnetic wave equations, 2019, Lecture Notes for the MFO seminar on wave phenomena http://www.math.kit.edu/ianm3/seite/mfoseminar/en.
[17] T. Roubíček, Nonlinear Partial Differential Equations with Applications, International Series of Numerical Mathematics (Birkhäuser Basel, 2006).
[18] M. Dreher and A. Jüngel, Nonlinear Analysis: Theory, Methods & Applications **75**(6), 3072–3077 (2012).